Bulletin of Geophysics and Oceanography Vol. XX, n. X, pp. XXX-XXX; Xxxxx 20xx
DOI 10.4430/bgo00532

Re-evaluation of *b*-value distributions in the Fethiye–Burdur Fault Zone (FBFZ), in south-western Turkey, for the period 2012-2024

T. Yeken[1], E. Öztürk[2] and T.S. Irmak[3]

[1] *Hereke Asım Kocabıyık Vocational School, Kocaeli University, Hereke, Kocaeli, Turkey*
[2] *Construction Department, Düzce University, Düzce, Turkey*
[3] *Dept. of Geophysical Engineering, Kocaeli University, Izmit –Kocaeli, Turkey*

(Received: 9 October 2024; accepted: 20 March 2026; published online: 8 September 2026)

ABSTRACT The Fethiye–Burdur Fault Zone (FBFZ) in south-western Turkey represents a seismically active region where complex interactions between tectonic stress and geothermal activity are associated with earthquake occurrence patterns, the understanding of which is improved by evolving seismic monitoring capabilities. This study analyses a declustered earthquake catalogue (2012–2024) to investigate spatiotemporal variations in completeness magnitude and *b*-values, providing insights into regional seismic hazard. The frequency-magnitude distribution yields a regional *b*-value of 0.82 ± 0.01, with temporal fluctuations showing precursory declines before significant earthquakes (e.g. the 2019 *M* 5.7 event), consistent with the interpretation of *b*-values as stress-sensitive parameters. Spatially, *b*-values increase from NE to SW, correlating with geothermal activity in the SW, where elevated values align with global geothermal/volcanic systems. Conversely, the Tefenni segment's persistently low *b*-value (~0.58) and historical quiescence may indicate that this is a mechanically important segment. These findings highlight the heterogeneous stress regime along the FBFZ, where geothermal fluids may modulate seismicity in the south-western sector while locked segments such as Tefenni accumulate strain under ongoing tectonic loading.

Key words: *b*-value, completeness magnitude, seismic hazard, Fethiye-Burdur Fault Zone.

1. Introduction

The Fethiye–Burdur Fault Zone (FBFZ) in south-western Turkey is a seismically active region that plays a critical role in the country's tectonic framework. As part of the broader Hellenic Arc and the complex deformation zone of the Anatolian Plate, the FBFZ has generated significant earthquakes throughout history, posing substantial seismic hazards to local populations and infrastructure (e.g. Polat *et al.*, 2008; Tan *et al.*, 2008; Bayrak and Bayrak, 2012; Bayrak *et al.*, 2017). In addition, the region's status as a major tourism hub further underscores the importance of understanding its seismic risk to support sustainable development and effective disaster preparedness.

The tectonic evolution of western Anatolia and the Aegean region is characterised by a combination of strike-slip tectonics and extensional deformation. This complex tectonic regime results from the westward escape of the Anatolian plate towards the Hellenic trench, driven by slab-edge processes at the northern boundary of the subducting African oceanic lithosphere (Şengör *et al.*, 1985; Taymaz *et al.*, 1991, 2007; Taymaz and Price, 1992; Irmak, 2013; Yolsal-Çevikbilen *et al.*, 2014). The interaction of these processes has created a network of structures, dominated by strike-slip faults in northern and central Anatolia, while normal faults with varying orientations prevail in western Anatolia and the Aegean region. The FBFZ lies at the intersection of these regions: western Anatolia, the Aegean, and central Anatolia (Fig. 1). This NE–SW trending, left-lateral strike-slip fault zone marks the western boundary of the Isparta Angle and is likely a continuation of the Pliny Fault Zone in the Hellenic arc (Dumont *et al.*, 1979; Taymaz and Price, 1992; Hall *et al.*, 2014; Doğan *et al.*, 2016; Elitez and Yaltırak, 2016; Alçiçek *et al.*, 2017; Kaymakçı *et al.*, 2018; Özkaptan *et al.*, 2018; Tosun *et al.*, 2021). Sarı *et al.* (2023) describe the FBFZ as approximately 300 km long and comprising four principal structural segments. These segments (from SW to NE) include: 1) the Fethiye segments, which have produced several significant earthquakes, including four with magnitudes greater than 6 during the instrumental-period (1 March 1926, M_s = 6.1; 24 and 25 April 1957, M_s = 6.9 and M_s = 7.1; 10 June 2012, M_w = 6.1); 2) the Gölhisar and Tefenni segments, approximately 50 and 40 km long, respectively, and characterised by a lower seismic activity compared to other segments; and 3) the Burdur segment which extends over 50 km and was the site of the 1914 M = 6.9 earthquake and the 1971 M_w = 5.9 event.

The *b*-value, a key parameter in earthquake statistics derived from the Gutenberg–Richter (GR) relationship (Gutenberg and Richter, 1944), provides valuable insights into stress accumulation and fault mechanics. Spatial variations in *b*-values can reflect differences in stress

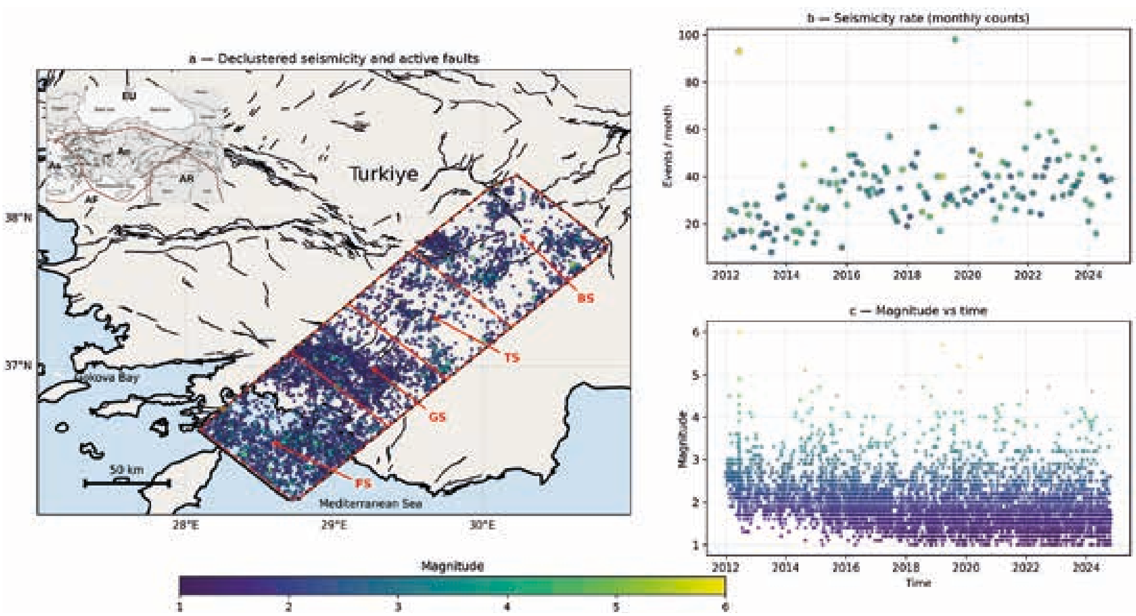

Fig. 1 - a) Declustered earthquake catalogue [M_L ≥ 1.0 earthquakes that occurred between 2 January 2012 and 31 December 2024 (KOERI, 2025)] and active faults within the study area. Earthquakes located inside the analysis polygon (red outline) are colour-coded according to magnitude. Black lines indicate fault segments [Fethiye segment (FS), Gölhisar segment (GS), Tefenni segment (TS), Burdur segment (BS)]. b) Monthly seismicity rate (number of events), point colours represent the maximum magnitude (max M) observed in each month. c) Magnitude–time distribution for the same dataset. In all panels, the colour scale represents earthquake magnitude and a common colour scale is used across all panels. The inset map shows the plate boundaries in and around Turkey: African (AF), Arabian (AR), Eurasian (EU), Anatolian (An), and the Aegean sea (As) plates. The black thick lines represent fault lines (Şaroğlu *et al.*, 1992).

distribution, fault maturity, and the presence of asperities or barriers along fault segments. Laboratory experiments and seismological observations demonstrate that *b*-values are inversely proportional to differential stress levels in the crust (e.g. Scholz, 1968, 2015; Wu *et al.*, 2018). Accordingly, regions characterised by high stress levels, where large earthquakes are more likely to occur, are typically associated with low *b*-values (Nanjo *et al.*, 2019).

Previous studies have further shown that *b*-values are sensitive to a range of crustal conditions directly or indirectly related to the stress state, including faulting style (Schorlemmer *et al.*, 2005; Petrucelli *et al.*, 2019), the presence of locked or creeping fault patches and material properties (Mogi, 1962; Wiemer and Wyss, 2000; Sobiesiak *et al.*, 2007; Ghosh *et al.*, 2008), and pore-pressure perturbations (Hainzl and Fischer, 2002; Bachmann *et al.*, 2012; Passarelli *et al.*, 2015; Shelly *et al.*, 2016). For example, normal faulting is generally associated with higher *b*-values, whereas reverse faulting tends to produce lower *b*-values (Amelung and King, 1997; Beauval and Scotti, 2004; Kulhánek, 2005; Schorlemmer *et al.*, 2004; Gulia *et al.*, 2010). A decline in *b*-value is commonly interpreted as an increase in tectonic stress preceding a significant seismic event (Scholz, 1968, 2015; Wyss, 1973; Schorlemmer *et al.*, 2005; Rivière *et al.*, 2018).

In addition, *b*-values tend to increase with greater material heterogeneity (Mogi, 1962; Sobiesiak, 2000) and are influenced by seismic velocity structure, with higher *b*-values observed in regions of low P-wave velocities and lower *b*-values in regions of high P-wave velocities (Ogata *et al.*, 1991; Salah *et al.*, 2007; Polat *et al.*, 2008). A positive relationship has also been documented between *b*-values and thermal conditions, such that elevated heat fluxes and thermal gradients are typically associated with higher *b*-values (Warren and Latham, 1970; Kisslinger and Jones, 1991; Utsu *et al.*, 1995).

Following the devastating 1999 Gölcük–Kocaeli (M_w7.4) and Düzce (M_w=7.2) earthquakes, Turkey significantly enhanced its seismological observation networks, leading to improved detection and accuracy in locating earthquakes of varying magnitudes, from microseismicity to major events (Alver *et al.*, 2019). These advancements have been particularly valuable for regions such as the FBFZ, where the denser seismic network now allows for more precise monitoring of spatiotemporal variations in *b*-values and completeness magnitude (*Mc*), both critical parameters for seismic hazard assessment. In south-western Turkey, including the FBFZ, this modernisation was accompanied by a progressive increase in station density after approximately 2010. This was performed primarily through the deployment of three-component broadband seismic stations operated by the Kandilli Observatory and Earthquake Research Institute (KOERI). In parallel, improvements in data acquisition, phase picking, and processing workflows contributed to enhanced hypocentral location quality and lower detection thresholds. Similar network-driven improvements and their impact on catalogue quality have been documented in other regions (e.g. Sandron *et al.*, 2023).

Given the FBFZ's complex tectonic setting, historical seismicity, and growing regional importance as both a population centre and tourism hub, this study was undertaken to provide a comprehensive, high-resolution analysis of the zone's contemporary seismic behaviour. By leveraging enhanced seismic networks deployed post-1999, we systematically investigate spatiotemporal variations in *b*-values and *Mc* across the fault segments, with particular focus on: 1) quantifying stress heterogeneity along the FBFZ's structurally diverse segments, 2) evaluating the interplay between geothermal activity and seismicity patterns in the SW, and 3) assessing the seismic potential of the historically quiescent, yet mechanically critical, Tefenni segment. Our findings not only advance the understanding of how tectonic, thermal, and network-detection factors collectively modulate earthquake occurrence in transtensional systems but also deliver actionable insights for updating seismic hazard models. This work is particularly relevant as the

FBFZ's dual role as a tectonic boundary and as a socioeconomically vital region necessitates science-based strategies to mitigate risks to infrastructure and communities, ultimately contributing to Turkey's resilience against future seismic disasters.

2. Methods

2.1. Seismic catalogue and declustering

This study utilises the seismic catalogue provided by KOERI, covering the period from 2000 to 2024. The catalogue is based on recordings from three-component broadband seismometers. Event detection, phase picking, hypocentral location, and magnitude determination follow standardised processing workflows implemented by KOERI. It should be noted that heterogeneous magnitude definitions (M_d, m_b, and M_L) were employed for earthquakes prior to 2012, whereas a uniform local magnitude scale (M_L) has been used consistently since 1 January 2012, ensuring improved catalogue homogeneity during the main analysis period (Cambaz *et al.*, 2019; Ali and Akkoyunlu, 2022).

To ensure that the statistical properties of seismicity are not biased by aftershock clustering, the earthquake catalogue was declustered prior to all analyses. We selected the Gardner and Knopoff (1974) declustering algorithm as our primary method following Perry and Bendick (2024). This decision was based on their demonstrated effectiveness in completely removing aftershock sequences across all tectonic environments, despite its tendency to be more conservative in event removal compared to other methods (e.g. Uhrhammer, Reasenberg, or ETAS-based algorithms). While this approach may eliminate more events than some modern alternatives, it provides the most consistent removal of dependent seismicity, a critical requirement for the reliable statistical analysis of seismicity parameters.

Gardner and Knopoff (1974) introduced a declustering algorithm that uses the spatial and temporal proximity of earthquakes to identify clusters of seismic events. In this method, earthquake events from a catalogue are arranged in descending order of magnitude. Starting with the largest event, space–time windows are defined around each event. The size of these windows depends on the earthquake's magnitude, with larger magnitudes leading to broader windows. Within each window, the largest event is classified as the mainshock, and smaller events are excluded as aftershocks. The window parameters are determined using the following equations proposed by Gardner and Knopoff (1974):

$$Log(T) = \alpha_1 M + \beta_1 \quad \text{(for time)} \tag{1}$$

$$Log(L) = \alpha_2 M + \beta_2 \quad \text{(for distance)} \tag{2}$$

In these equations, T represents the temporal window (in days) and L represents the spatial window (in kilometres) used for declustering. M denotes the earthquake magnitude. Coefficients α_1, β_1, α_2, and β_2 are empirical constants defined by Gardner and Knopoff (1974), which control the magnitude-dependent scaling of the space–time windows.

Following declustering, the number of earthquakes in the 2012–2024 catalogue was reduced from 13,360 to 5,272. The declustered catalogue, comprising exclusively independent seismic events, served as the dataset for all subsequent analyses, including the estimation of *Mc* and *b*-values.

2.2. Completeness magnitude and b*-value*

Mc a critical parameter in seismic studies, represents the lowest magnitude above which all earthquakes in a given catalogue are reliably recorded. It plays a fundamental role in accurately assessing seismic activity by ensuring that the dataset used in seismic hazard analysis is free from bias due to missing smaller events. An improperly determined *Mc* can lead to an underestimation of earthquake recurrence rates and distort the frequency-magnitude distribution (FMD), especially in regions where smaller earthquakes are frequent (Wiemer and Wyss, 1997). *Mc* is influenced by several factors, such as the density and sensitivity of the seismic network, regional geological conditions, and advancements in seismic instrumentation over time. As seismic networks improve, *Mc* tends to decrease, allowing for more comprehensive earthquake catalogues. Proper determination of *Mc* is essential for high-quality seismic hazard assessments, as it guarantees that the catalogue captures all significant seismic events, providing a reliable foundation for understanding seismicity patterns and forecasting future risks.

To ensure robust and reproducible results, all parameter calculations were performed using ZMAP7 (Wiemer, 2001), a widely used MATLAB toolbox designed for statistical seismicity analysis. All analyses were conducted on the declustered catalogue to minimise potential biases associated with aftershock sequences while preserving the statistical characteristics of the background seismicity. This framework was used to estimate key parameters, including *Mc* and *b*-values.

Initial analysis revealed significant discrepancies in the FMD for pre-2012 events, particularly for *M* > 4 earthquakes, where the scaling relationship exhibited poor fit (Fig. 2). Although the post-2012 catalogue exhibits improved magnitude homogeneity, a systematic deviation from the expected GR scaling remains near the estimated *Mc* completeness threshold. To further evaluate the completeness characteristics of the catalogue, the FMD was analysed using the maximum curvature method. Following the approach of Woessner and Wiemer (2005), a small correction

a) b)

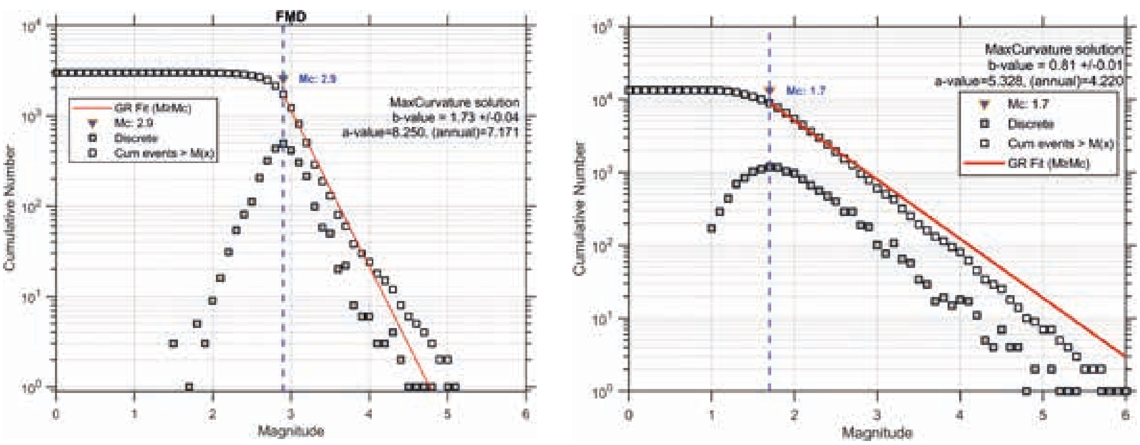

Fig. 2 - FMDs and GR fits for the studied catalogue. a) For the 2000–2011 catalogue period (pre-magnitude standardisation), the FMD exhibits a clear deviation from the linear GR relationship at larger magnitudes, reflecting departures from ideal GR scaling. b) For the post-standardisation period (2012–2024), the FMD shows improved overall linearity; however, systematic deviations from the GR trend persist at higher magnitudes, indicating potential changes in the relative scaling behaviour of the catalogue. The *a*-value is reported as an annualised seismicity rate, normalised to one year of observation.

of +0.2 magnitude units was added to the initial *Mc* estimate to obtain a more stable GR fit. The resulting corrected FMD (Fig. S2 in the Supplementary materials) confirms that the catalogue follows the expected scaling behaviour above the adjusted *Mc*. Consequently, all subsequent analyses were restricted to the homogenised post-2012 catalogue (*N* = 13,360 events), which was subsequently declustered to obtain a catalogue of 5,272 independent earthquakes.

In the context of *b*-value estimation and seismic quietness analysis, utilising the highest number of data points is crucial for producing reliable and statistically robust results. Therefore, determining *Mc* is a fundamental step in these analyses and is typically achieved by examining the distribution of earthquake counts by magnitude, where *Mc* is approximated using the maximum of the first derivative of the FMD (Wyss *et al.*, 1999; Wiemer and Wyss, 2000). The maximum curvature (MAXC) method was selected as an objective and widely used first-order estimator of *Mc*, particularly suitable for large regional catalogues. The MAXC method identifies *Mc* as the magnitude corresponding to the point of MAXC, calculated as the maximum value of the first derivative of the FMD. Generally, the *Mc* obtained with the MAXC method, which is typically used as the initial condition in many of the algorithms introduced later, corresponds to the magnitude with the highest event frequency in the FMD.

To systematically account for temporal variations in seismic network sensitivity, we calculated *Mc* and *b*-values as a function of time using a moving-window approach. The analysis was performed using windows defined by a fixed number of events, with a 4% step size between successive windows, corresponding to a 96% overlap. This configuration smooths the temporal evolution of the *b*-value time series while balancing statistical robustness and minimising artificial correlation between adjacent windows. A minimum threshold of 20 events above the *Mc* was imposed solely as a lower bound to permit *b*-value computation during periods of reduced seismicity and does not represent the effective window size. As shown in Fig. S1 of the Supplementary materials, the effective number of events contributing to each window is substantially larger, with most windows containing approximately 50–120 events above the *Mc* and a peak around 70–100 events. This confirms that the temporal *b*-value estimates are predominantly based on statistically robust sample sizes rather than near-minimum counts, and that short windows are interpreted conservatively in terms of relative variations rather than absolute values. Uncertainty quantification was achieved through 200 bootstrap iterations for each window, providing confidence bounds on the estimated *b*-values. This completeness-controlled framework provides a consistent basis for subsequent *b*-value estimation, ensuring that observed spatiotemporal variations reflect physical changes in the stress regime and seismicity patterns rather than artefacts of catalogue incompleteness. Although some studies suggest that wider magnitude ranges can further stabilise GR fits, the maximum-likelihood method is known to provide robust *b*-value estimates even when the usable magnitude range or sample size is limited, provided that events above the magnitude *Mc* are used, which is commonly the case for regional earthquake catalogues (Woessner and Wiemer, 2005; Nava *et al.*, 2017; Pisarenko *et al.*, 2023).

An empirical scale law for the magnitude–earthquake number relationship of earthquake occurrences was defined by Gutenberg and Richter (1944). This form is the fundamental relation of earthquake statistics and is given by the following equation:

$$log_{10} N(M) = a - bM \tag{3}$$

In this equation, *N(M)* is the cumulative number of events in a given time period with magnitude greater than, or equal to, *M*. The *b*-value is obtained from the slope of the FMD, whereas the *a*-value reflects the overall seismicity rate. Changes in the *a*-value for different seismic areas are related to the duration of the earthquake catalogue, the size of the study area, and the number of recorded earthquakes (Popandopoulos and Lukk, 2014).

The *b*-value was estimated using the maximum-likelihood method, which provides a robust and widely adopted approach for characterising the FMD slope (Aki, 1965; Utsu, 1966). For discretised magnitude data, the formulation proposed by Aki (1965), and later refined by Bender (1983), was employed. The *b*-value uncertainty was calculated following the formulation of Shi and Bolt (1982):

$$b = \frac{log_{10}(e)}{\left[(\bar{M}) - \left(Mc - \frac{\Delta M_{bin}}{2}\right)\right]} \tag{4}$$

$$\delta b = 2.30 \times b^2 \sqrt{\sum_{i=1}^{n} \frac{(M_i - \bar{M})}{n_s(n_s - 1)}} \tag{5}$$

where $\bar{M}$ is the mean magnitude of the binned event magnitudes, M_c is the completeness magnitude, ΔM_{bin} = 0.1 is the magnitude bin width, M_i denotes the magnitude of the *i*-th event, and n_s is the number of events above M_c used in the estimation. The quantity *δb* denotes the analytical standard error of the estimated *b*-value and was calculated using Eq. (5) following Shi and Bolt (1982). Bootstrap uncertainty was assessed separately using 200 resamples for each moving window. For the time-series analysis, windows containing 500 events were shifted by 4% of the window size between successive estimates, corresponding to a 96% overlap. A minimum of 20 events above M_c was required for computation.

In addition to the temporal analysis described above, the spatial variability of *b*-values was investigated using the mapping tools implemented in ZMAP7 software (Wiemer and Wyss, 1997; Wiemer, 2001). In this approach, *b*-values are calculated at regularly distributed grid nodes across the study area using the nearest earthquakes surrounding each node. For the spatial analysis, the 500 nearest events were used to ensure statistically stable estimates, while a minimum requirement of 20 earthquakes above the local *Mc* was imposed for each node. Because neighbouring nodes share partially overlapping earthquake datasets, the resulting spatial distribution of *b*-values represents a spatially smoothed field rather than strictly independent estimates at each grid node. Such node-based approaches are widely used in spatial seismicity analyses to identify variations in stress conditions and fault behaviour (e.g. Tormann *et al.*, 2014).

3. Results and discussion

Upon analysing the declustered earthquake catalogue for the period between 2012 and 2024, a clear temporal decrease in the *Mc* is observed, from approximately 2.4 to 1.8 (Fig. 3). This reduction in *Mc* is primarily attributed to the substantial expansion and densification of the regional seismic monitoring network, particularly through the deployment of additional broadband stations and improvements in overall network sensitivity. Enhanced station coverage and data quality have increased the detection capability for smaller-magnitude earthquakes, resulting in progressively lower *Mc* values. The decline in *Mc* is most pronounced between 2012 and 2018, after which *Mc* stabilises at around 1.8, indicating that the seismic network has

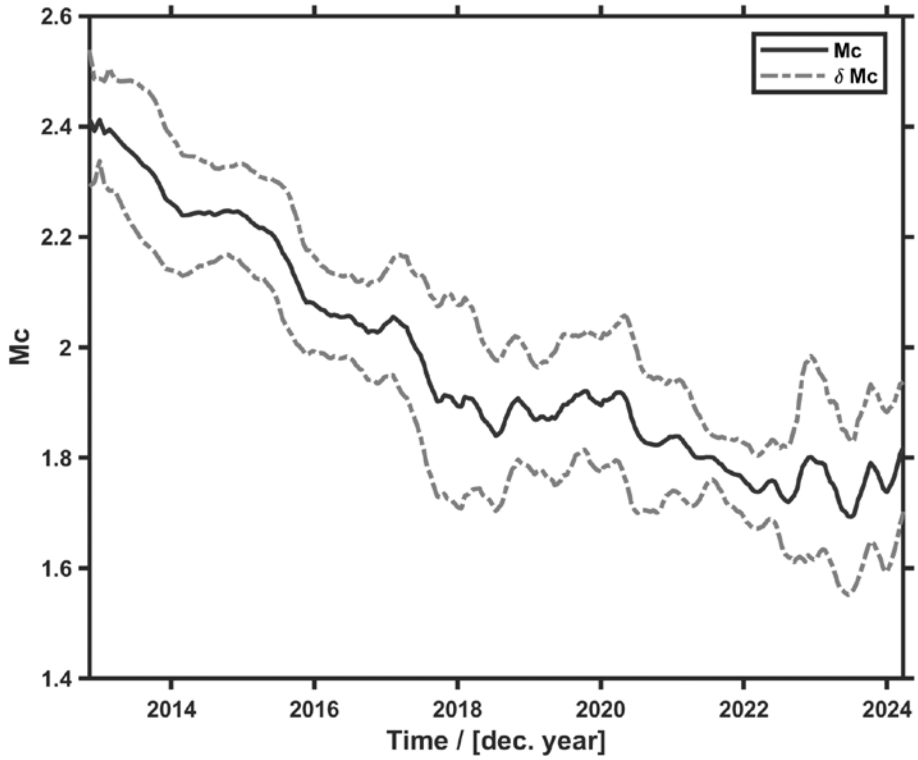

Fig. 3 - Temporal evolution of the *Mc* estimated from the declustered earthquake catalogue for the period 2012–2024. Solid black line shows *Mc*, while dashed lines indicate its uncertainty bounds. The pronounced decrease in *Mc* between 2012 and 2018 coincides with improvements in seismic network density and detection capability, whereas the subsequent stabilisation around *Mc* ≈ 1.8 reflects a mature monitoring configuration.

reached a mature configuration in which further significant reductions in *Mc* are unlikely under the current monitoring configuration.

A comparative analysis with previous studies such as the work by Bayrak *et al.* (2017) highlights differences in the *Mc* values over time. Bayrak *et al.* (2017) reported an *Mc* value of 2.8 for a comparable region, using a catalogue covering the years 1900–2010. It is worth noting that the magnitude scale used in such study was surface wave magnitude (*Ms*), which differs from the local magnitude (M_L) employed in the current study. Nevertheless, Tan (2020) determined the *Mc* value to be between 3.0 and 3.2 for the region within the FBFZ in his study, utilising earthquake data from 1900 to 2017 for the entirety of Turkey. The distinction between different magnitudes can affect the interpretation of results, as different magnitude scales capture seismic energy differently, particularly for events at varying depths and distances from seismic stations. This underscores the importance of considering the magnitude type when comparing *Mc* values as well as *b*-values across different studies. The observed decline in *Mc* over time, and its subsequent stabilisation, reflects both the evolution of seismic monitoring capabilities and the growing sophistication of earthquake catalogues in the region. As the seismic network continues to evolve, ongoing monitoring of *Mc* is essential to ensure that the completeness of the earthquake catalogue remains reliable for accurate seismic hazard assessments.

The magnitude–earthquake number relationship analysis results for the time period 2012–2024 are shown in Fig. 4. The *a*-value is a parameter primarily associated with the seismicity rate, area, and time-window of the investigation. While the *a*-value reflects the overall earthquake

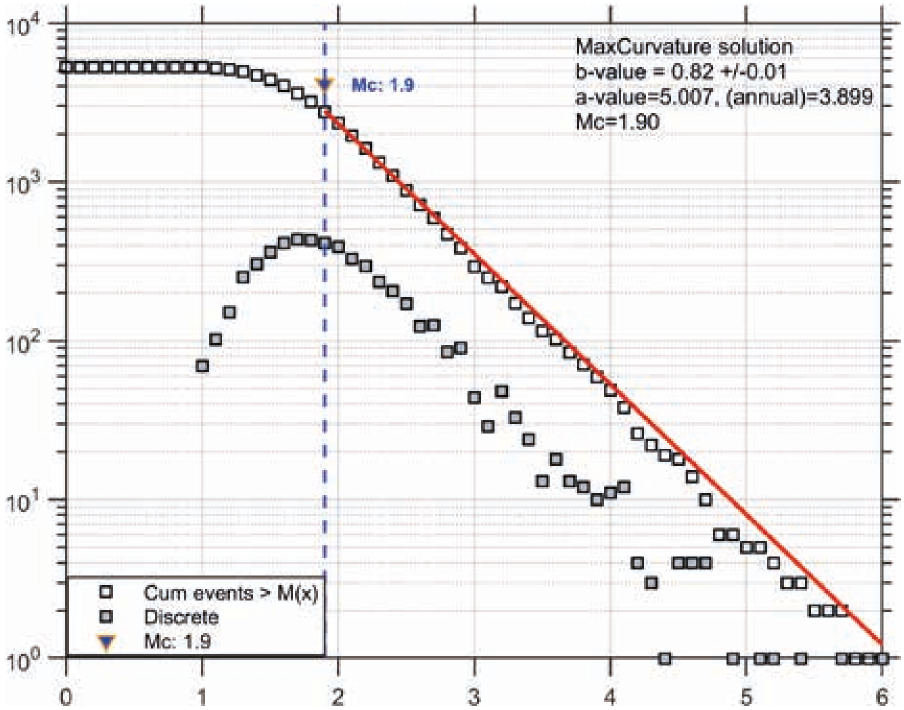

Fig. 4 - FMD graph obtained using the declustered catalogue (2012–2024, 5,272 events). The straight line is the best fit by Eq. (3). The *a*-value is reported as an annualised seismicity rate, normalised to one year of observation.

productivity, the *b*-value offers deeper insights into the relative frequency of large and small earthquakes, making it more useful for understanding earthquake occurrence patterns. Typically, the *b*-value hovers around the unity (1.0) over extended periods of time and large geographic regions. However, it exhibits significant variability over shorter timeframes and in more localised areas due to a variety of factors.

The declustered final earthquake catalogue produced *a*- and *b*-values of 5.01 and 0.82 ± 0.01, respectively. Türe *et al.* (2021) calculated the *b*-value as 0.63 ± 0.01 on the FBFZ in their analysis, lower than our results. However, our results are consistent with findings from Bayrak and Bayrak (2012) and Bayrak *et al.* (2017), who reported *b*-values between 0.71 and 0.86 in a similar geographical subdivision of the region.

A comparative analysis between the clustered and declustered catalogues reveals systematic differences in *b*-value estimations, consistent with established seismological principles where declustering typically yields lower *b*-values due to the removal of aftershock sequences that disproportionately increase the frequency of smaller-magnitude events (Mizrahi *et al.*, 2021). In this study, the clustered catalogue produced a *b*-value of 0.88 (Fig. S2 in the Supplementary materials), while the declustered version yielded 0.82 (Fig. 4), a marginal but statistically significant difference of 6.8%. This relatively small variance (< 7%) suggests that the mainshock-dominated seismicity in the FBFZ exhibits intrinsic stress conditions that are robust to the specific catalogue processing applied in this study, particularly the declustering procedure. Consequently, all subsequent analyses were conducted using the declustered catalogue, as it provides a more conservative representation of tectonic stress while maintaining fidelity to the region's fundamental seismogenic characteristics.

While the comparison between the clustered and declustered catalogues indicates only a minor difference in the overall *b*-value estimates, it is important to note that declustering effects may become more pronounced when short temporal windows are considered, particularly in the immediate vicinity of large earthquakes. In such cases, the removal of aftershock sequences can locally reduce the effective number of events, potentially amplifying short-term fluctuations in *b*-value. For this reason, our interpretation of the time-dependent *b*-value results emphasises relative temporal trends rather than individual window-specific values, especially around major events. A supplementary analysis further illustrates that although short-term deviations between clustered and declustered catalogues may occur, the overall temporal patterns remain consistent.

To further assess the impact of declustering on short temporal windows, we explicitly quantified the time-dependent difference between clustered and declustered *b*-values (Fig. 5). Although the clustered catalogue generally yields slightly higher *b*-values due to the inclusion of aftershock sequences, the overall temporal evolution of *b*-values remains remarkably similar in both cases. The time-dependent difference $\Delta b(t) = b$_clustered − b_declustered demonstrates that declustering-related effects are event-dependent: short-lived amplifications occur in the vicinity of some moderate-to-large earthquakes, whereas for others $\Delta b(t)$ remains close to zero or even decreases slightly. These transient and oscillatory responses likely reflect variations in aftershock productivity, detection thresholds, and the interaction between fixed-event windowing and post-seismic seismicity. Importantly, no persistent or systematic bias is introduced by the declustering procedure, indicating that the observed temporal *b*-value variations primarily reflect genuine changes in seismicity rather than artefacts of catalogue processing.

An analysis of the temporal variation in the *b*-value reveals pronounced fluctuations over time (blue line in Fig. 5), rather than a monotonic trend. Following an overall increase during the early part of the study period (2012–2013), the *b*-value exhibits a general tendency towards lower values between 2013 and 2015, although this interval is characterised by short-term variability rather than a strictly linear decline. A decrease in *b*-value occurs around the time of the 24 August 2014 M_w 5.1 earthquake, but the recovery that follows indicates a dynamic response rather than a persistent shift.

Subsequently, *b*-values reach relatively elevated levels during 2016–2017 before declining again towards lower values during the 2018–2019 period. The M_w 5.7 earthquake of 20 March 2019 occurs during this broader phase of reduced *b*-values, although the minimum values observed around this time are part of a wider interval of depressed *b*-values rather than a single, sharply defined minimum. After mid-2019, the *b*-value enters a renewed phase of moderate increase and fluctuation, remaining within a range of approximately 0.83–0.95 through the end of 2024.

Based on the declustered earthquake catalogue, the decrease in *b*-value prior to significant seismic events has been discussed in the literature as a potential stress-sensitive indicator with probabilistic relevance to earthquake occurrence. Studies by Wu and Chiao (2006) and Wu *et al.* (2008) in Taiwan suggest that a low seismicity rate and a declining *b*-value can serve as predictive indicators, reflecting a reduction in seismicity before large earthquakes. From this perspective, the decline in the *b*-value observed prior to the 20 March 2019 earthquake may indicate heightened stress accumulation leading up to this event. However, the absence of seismic events in other regions exhibiting *b*-value declines suggests that such reductions do not universally indicate an imminent seismogenic state, highlighting the potential influence of aseismic deformation or heterogeneous stress accommodation. It should be emphasised that *b*-value decreases are not restricted to the pre-seismic phase and may persist into the post-seismic period. Following a mainshock, processes such as stress redistribution, aftershock sequence development, and possible aseismic deformation can maintain locally elevated differential stress levels, delaying the recovery of *b*-values to background conditions. Consequently, *b*-value evolution should be interpreted within the broader context of

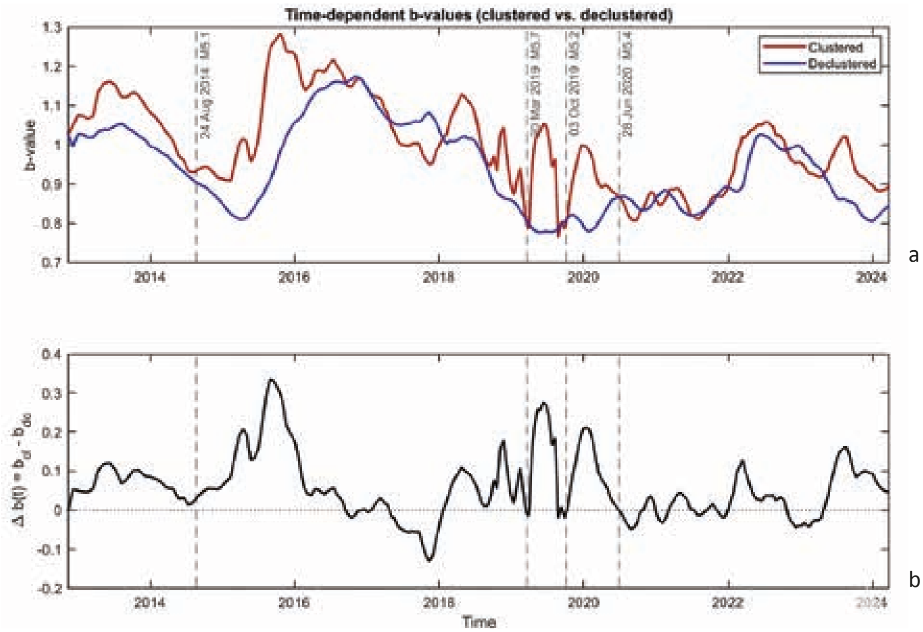

Fig. 5 - Time-dependent comparison of *b*-values derived from clustered and declustered earthquake catalogues. a) Temporal evolution of *b*-values estimated using identical analysis parameters for the clustered (red) and declustered (blue) catalogues. Vertical dashed lines indicate the occurrence times of moderate-to-large earthquakes ($M \geq 5$) in the study area. While clustered *b*-values are systematically slightly higher due to the contribution of aftershock sequences, both time series exhibit highly similar long-term temporal patterns. b) Time-dependent difference between clustered and declustered *b*-values, defined as $\Delta b(t) = b\_clustered - b\_declustered$. Positive values indicate higher *b*-values in the clustered catalogue. Transient, event-dependent deviations are observed in the vicinity of some earthquakes, whereas for others $\Delta b(t)$ remains close to zero or decreases slightly. The absence of persistent offsets demonstrates that declustering effects are short-lived and do not introduce systematic bias into the temporal *b*-value trends.

the seismic cycle rather than as a strictly premonitory signal.

The spatial distribution of *b*-values in the FBFZ between 2012 and 2024 exhibits notable variability (Fig. 6). The *b*-value ranges between a minimum of 0.53 and a maximum of 1.57. In the south-western part of the Burdur Lake, the *b*-value is as low as 0.58, around Fethiye Bay, the *b*-value reaches 1.28. The data indicate a general trend of increasing *b*-values from NE to SW. Similarly, Akar *et al.* (2022), in their analysis using earthquakes occurring in the Bodrum and Fethiye regions, showed that the *b*-value on the FBFZ increased from NE to SW.

The spatial variation in *b*-values within the study area can be attributed to multiple factors, among which geothermal activity appears to play a significant role, particularly in the south-western region where geothermal springs with temperatures ranging from 20 °C to 49 °C are widespread. The elevated *b*-values observed in this sector are consistent with those documented in other geothermal and volcanic regions worldwide, such as the Geysers [1.0–2.9: Leptokaropoulos (2020)] and Coso [1.0–1.8: Kaven *et al.* (2012)] geothermal fields in the USA, as well as volcanic systems like Mount St. Helens [0.5–1.5: Wiemer and McNutt (1997)], Yellowstone [0.6–1.5: Farrell *et al.* (2009)], and Popocatépetl [0.5–2.9: Garza-Girón (2014) and Rodríguez-Pérez *et al.* (2021)]. These thermal anomalies likely contribute to the higher *b*-values by altering crustal rheology and stress distribution, a phenomenon also noted by Salah *et al.* (2007), who reported a correlation between high P-wave velocities (indicative of low *b*-values) and specific structural segments, including the NE of the Burdur Lake and the junction of the Gölhisar and Tefenni fault segments.

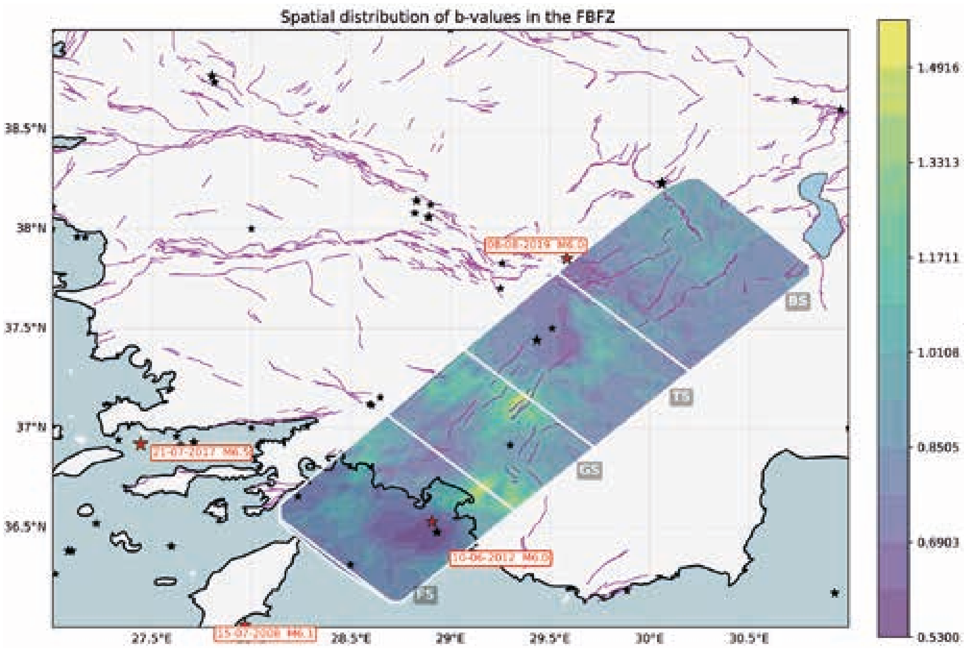

Fig. 6 - Spatial distribution of the *b*-value within the study area, calculated from the declustered earthquake catalogue. The analysis region is subdivided into four fault-related segments along the principal structural trend: Fethiye segment (FS), Gölhisar segment (GS), Tefenni segment (TS), and Burdur segment (BS) (after Sarı *et al.*, 2023). Magenta lines represent mapped active faults compiled from Şaroğlu *et al.* (1992). Earthquakes with magnitudes 5 ≤ *M* <6 are indicated with black stars, while earthquakes with *M* > 6 that occurred between 1990 and 2024 are marked with red stars. Red labels indicate the occurrence dates of the corresponding *M* > 6 events. The colour scale represents spatial variations in the *b*-value.

It should be noted that the spatial *b*-value patterns shown in Fig. 6 represent smoothed estimates at the segment scale, while localised stress heterogeneities associated with low seismicity zones, such as the Tefenni segment, are more clearly resolved through node-based analyses. Beyond geothermal influences, the spatial distribution of *b*-values provides critical information about regional stress accumulation and seismic potential. Empirical studies have demonstrated that persistently low *b*-values are commonly associated with elevated stress levels and may precede major earthquakes, serving as potential indicators of heightened stress concentrations (Ogata and Katsura, 1993; Wyss *et al.*, 2000). In particular, Main *et al.* (1989) suggested that *b*-values approaching ~0.5 may signify critical stress conditions conducive to large seismic events. This observation is most clearly expressed in the Fethiye segment, where persistently low *b*-values form laterally continuous patches, indicating a region of enhanced and sustained stress accumulation. In contrast, the spatially smoothed *b*-value map (Fig. 6) shows predominantly moderate *b*-values (~0.9–1.1) at the segment scale along the Gölhisar, Tefenni, and Burdur segments. While localised low *b*-value minima are identified within these segments through node-based analyses, they are spatially limited and do not form laterally continuous zones comparable to those observed in the southern Fethiye segment. This pattern suggests that stress accumulation along the FBFZ is highly heterogeneous, with persistent low *b*-values concentrated in the Fethiye segment and more localised, transient stress concentrations distributed elsewhere along the fault system. In particular, the Tefenni segment appears moderately stressed at the segment scale, although isolated low *b*-value nodes identified analytically suggest the presence of localised stress concentrations that are not visually dominant in the smoothed map.

4. Conclusions

The *Mc* decline observed from 2.4 to 1.8 primarily reflects improvements in seismic network density and detection capability, while its stabilisation after ~2018 indicates a consistent level of monitoring performance. Further reductions in *Mc* would likely require substantial changes in station density or instrumentation rather than incremental upgrades.

Temporal *b*-value variations exhibit correlations with significant seismic events, most notably a decline preceding the 2019 M_w 5.7 earthquake, consistent with observations from other tectonic regions. However, these variations are interpreted in a probabilistic rather than deterministic framework, as not all *b*-value decreases culminate in large earthquakes. Spatially, *b*-values increase from NE to SW, a trend that suggests geothermal systems may locally influence crustal rheology and stress conditions. Localised zoned persistently low *b*-values observed in parts of the FBFZ, particularly within localised patches, indicate heterogeneous stress accumulation rather than uniform segment-scale behaviour. Although the Tefenni segment has remained relatively quiescent during the instrumental period, its locally low *b*-values highlight the need for continued monitoring, as such segments may play a mechanically important role in controlling future rupture processes. Beyond the specific findings presented in this study, the results also contribute to a broader understanding of seismic hazard in the FBFZ. By constructing a completeness-corrected earthquake catalogue and analysing the spatiotemporal variability of *b*-values, this work provides new insights into the spatial heterogeneity of stress conditions and the segmentation of seismic activity along the fault system. Such information is essential for improving the characterisation of earthquake occurrence patterns in complex extensional tectonic environments. The results therefore contribute to ongoing efforts to refine regional seismic hazard assessments and to better understand the processes controlling earthquake generation in the south-western Anatolian tectonic regime.

Acknowledgments. The authors thank the editor and three anonymous reviewers for their constructive comments and insightful suggestions, which helped to improve the clarity and quality of this manuscript. We would like to thank Kocaeli University Research Fund (KOU-BAP).
Supplementary materials. Additional figures are available at the BGO website https://bgo.ogs.it.

REFERENCES

Ali S.M. and Akkoyunlu M.F.; 2022: *Statistical analysis of earthquake catalogs for seismic hazard studies around the Karliova Triple Junction (eastern Turkey)*. J. Afr. Earth Sci., 186, 104436.

Akar F., Akkoyunlu M.F. and Bilim F.; 2022: *The spatial analysis of b values of the area between Bodrum and Fethiye districts, the south-western Anatolia, Turkey.* Mühendislik Bilimleri ve Tasarım Dergisi, 10, 238-246.

Aki K.; 1965: *Maximum likelihood estimate of b in the formula logN = a − bM and its confidence limits.* Bull. Earthq. Res. Inst., 43, 237-239.

Alçiçek H., Wesselingh F.P., Alçiçek M.C., Jiménez-Moreno G., Feijen F.J., van den Hoek Ostende L.W., Mayda S. and Tesakov A.S.; 2017: *A multiproxy study of the early Pleistocene palaeoenvironmental and palaeoclimatic conditions of an anastomosed fluvial sequence from the Çameli Basin (SW Anatolia, Turkey).* Palaeogeogr. Palaeoclimatol. Palaeoecol., 467, 232–252. doi:10.1016/j.palaeo.2016.08.019.

Alver F., Kılıçarslan Ö., Kuterdem K., Türkoğlu M. and Şentürk M.D.; 2019: *Seismic Monitoring at the Turkish National Seismic Network (TNSN).* Summ. Bull. Int. Seismol. Cent., 53, 41-58.

Amelung F. and King G.; 1997: *Earthquake scaling laws for creeping and non-creeping faults.* Geophys. Res. Lett., 24, 507-510.

Bachmann C., Wiemer S., Goertz-Allmann B. and Woessner J.; 2012: *Influence of pore pressure on the size distribution of induced earthquakes.* Geophys. Res. Lett., 39, L09302.

Bayrak Y. and Bayrak E.; 2012: *An evaluation of earthquake hazard potential for different regions in Western Anatolia using the historical and instrumental earthquake data.* Pure Appl. Geophys., 169, 1859-1873.

Bayrak E., Yılmaz Ş. and Bayrak Y.; 2017: *Temporal and spatial variations of Gutenberg-Richter parameter and fractal dimension in Western Anatolia, Turkey.* J. Asian Earth Sci., 138, 1-11.

Bender B.; 1983: *Maximum likelihood estimation of b values for magnitude grouped data.* Bull. Seismol. Soc. Am., 73, 831-851.

Beauval C. and Scotti O.; 2004: *Quantifying sensitivities of PSHA for France to earthquake catalog uncertainties, truncation of ground-motion variability, and magnitude limits.* Bull. Seismol. Soc. Am., 94, 1579-1594.

Cambaz M.D., Turhan F., Yılmazer M., Kekovalı K., Necmioğlu Ö. and Kalafat D.; 2019: *A review on Kandilli Observatory and Earthquake Research Institute (KOERI) seismic network and earthquake catalog: 2008–2018*. Adv. Geosci., 51, 15-23.

Doğan B., Irmak T.S., Karakaş A. and Kalafat D.; 2016: *Seismotectonic content by the source parameters of the 10 June 2012 Ölüdeniz-Fethiye (Dodecanese Islands) Mw 6.1 earthquake and aftershocks (south-western Turkey)*. Acta Geod. Geophys., 51, 15-41.

Dumont J.F., Poisson A. and Sahinci A.; 1979: *Sur l'existence de coulissements sinistres recentes a l'extermité orientale de l'arc ageen (sud-ouest de la Turquie).* C. R. Acad. Sci. Paris, 289, 261-264.

Elitez İ. and Yaltırak C.; 2016: *Miocene to Quaternary tectonostratigraphic evolution of the middle section of the Burdur-Fethiye Shear Zone, south-western Turkey: Implications for the wide inter-plate shear zones.* Tectonophysics, 690, 336-354.

Farrell J.M., Husen S. and Smith R.B.; 2009: *Earthquake swarm and b-value characterization of the Yellowstone volcano-tectonic system.* J. Volcanol. Geoth. Res., 188, 260-276.

Gardner J. and Knopoff L.; 1974: *Is the sequence of earthquakes in southern California, with aftershocks removed, poissonian?* Bull. Seismol. Soc. Am., 64, 1363-1367.

Garza-Giron R.; 2014: *Distribución del valor b debajo del volcán Popocatépetl y su relación con la estructura de la cámara magmática*. Bachelor's degree thesis. Universidad Nacional Autónoma de México, Facultad de Ingeniería, 162 p.

Ghosh A., Newman A.V., Thomas A.M. and Farmer G.T.; 2008: *Interface locking along the subduction megathrust from b-value mapping near Nicoya Peninsula*. Costa Rica. Geophys. Res. Lett., 35, L01301.

Gulia L., Wiemer S. and Schorlemmer D.; 2010: *Asperity-based earthquake likelihood models for Italy.* Ann. Geophys., 53, 63-75.

Gutenberg B. and Richter C.F.; 1944: *Frequency of earthquakes in California*. Bull. Seismol. Soc. Am., 34, 185-188.

Hall J., Aksu A.E., Elitez İ., Yaltırak C. and Çifçi G.; 2014: The Fethiye–Burdur Fault Zone: a component of upper plate extension of the subduction transform edge propagator fault linking Hellenic and Cyprus Arcs, Eastern Mediterranean. Tectonophysics, 635, 80-99.

Hainzl S. and Fischer T.; 2002: *Indications for a successively triggered rupture growth underlying the 2000 earthquake swarm in Vogtland/NW Bohemia*. J. Geophys. Res., 107, B12.

Irmak T.S.; 2013: *Focal mechanisms of small-moderate earthquakes in Denizli Graben (SW Turkey).* Earth Planets Space, 65, 943-955.

Kaven J.O., Hickman S.H. and Davatzes N.C.; 2012: *Mapping of Fluid Compartments with Micro-Seismicity and Seismic Velocities Within the Coso Geothermal Field, California.* In: *Proc. 37th Workshop on Geothermal Reservoir Engineering*. Stanford University, Stanford, California.

Kaymakcı N., Langereis C., Özkaptan M., Özacar A.A., Gülyüz E., Uzel B. and Sözbilir H.; 2018: *Paleomagnetic evidence for upper plate response to a STEP fault, SW Anatolia.* Earth Planet. Sci. Lett., 498, 101-115.

Kisslinger C. and Jones L.M.; 1991: *Properties of aftershock sequences in southern California.* J. Geophys. Res., 96, 11947-11958.

Kandilli Observatory and Earthquake Research Institute (KOERI); 2025: Earthquake database. <www.koeri.boun.edu.tr/sismo/zeqdb/>. Last accessed 15 March 2025.

Kulhánek O.; 2005: *Seminar on b-value*. Department of Geophysics, Charles University.

Leptokaropoulos K.; 2020: *Magnitude distribution complexity and variation at the Geysers geothermal field.* Geophys. J. Int., 222, 893-906, doi: 10.1093/gji/ggaa208.

Main I., Meredith P. and Jones C.; 1989: *A reinterpretation of the precursory seismic b-value anomaly from fracture mechanics*. Geophys. J. Int., 96, 131-138.

Mizrahi L., Nandan S. and Wiemer S.; 2021: *Embracing data incompleteness for better earthquake forecasting*. J. Geophys. Res. Solid Earth, 126, e2021JB022379.

Mogi K.; 1962: *On the time distribution of aftershocks accompanying the recent major earthquakes in and near Japan.* Bull. Earthq. Res. Inst., 40, 107-124.

Nanjo K.Z., Izutsu J., Orihara Y., Kamogawa M. and Nagao T.; 2019: *Changes in seismicity pattern due to the 2016 Kumamoto earthquakes identify a highly stressed area on the Hinagu Fault Zone.* Geophys. Res. Lett., 46, 9489-9496.

Nava F.A., Márquez-Ramírez V.H., Zúñiga F.R., Ávila-Barrientos L. and Quinteros C.B.; 2017: *Gutenberg-Richter b-value maximum likelihood estimation and sample size.* J. Seismol., 21, 127–135.

Ogata Y., Imoto M. and Katsura K.; 1991: *3-D spatial variation of b-values of magnitude-frequency distribution beneath the Kanto District,* Japan. Geophys. J. Int., 104, 135-146.

Ogata Y. and Katsura K.; 1993: *Analysis of temporal and spatial heterogeneity of magnitude frequency distribution inferred from earthquake catalogues.* Geophys. J. Int., 113, 727-738.

Özkaptan M., Kaymakcı N., Langereis C.G., Gülyüz E., Özacar A.A., Uzel B. and Sözbilir H.; 2018: *Age and kinematics of the Burdur Basin: Inferences for the existence of the Fethiye Burdur Fault Zone in SW Anatolia (Turkey).* Tectonophysics, 744, 256-274.

Passarelli L., Hainzl S., Cesca S., Maccaferri F., Mucciarelli M., Roessler D., Corbi F., Dahm T. and Rivalta E.; 2015: *Aseismic transient driving the swarm-like seismic sequence in the Pollino range, Southern Italy*. Geophys. J. Int., 201, 1553-1567.

Perry M. and Bendick R.; 2024: *A comparative analysis of five commonly implemented declustering algorithms.* J. Seismol., 28, 829-842.

Petruccelli A., Schorlemmer D., Tormann T., Rinaldi A.P., Wiemer S., Gasperini P. and Vannucci G.; 2019: *The influence of faulting style on the size-distribution of global earthquakes*. Earth Planet. Sci. Lett., 527, 115791.

Pisarenko V.F., Skorkina A.A. and Rukavishnikova T.A.; 2023: *Choosing the magnitude range for estimating the b-value.* J. Volcanol. Seismol., 17, 75-82.

Polat O., Goek E. and Yilmaz D.; 2008: *Earthquake hazard of the Aegean extension region (West Turkey).* Turk. J. Earth Sci., 17, 593-614.

Popandopoulos G.A. and Lukk A.A.; 2014: *The depth variations in the b-value of frequency-magnitude distribution of the earthquakes in the Garm region of Tajikistan.* Izv. Phys. Solid Earth, 50, 273-288.

Rivière J., Lv Z., Johnson P.A. and Marone C.; 2018: *Evolution of b-value during the seismic cycle: Insights from laboratory experiments on simulated faults.* Earth Planet. Sci. Lett., 482, 407-413.

Rodríguez-Pérez Q., Monterrubio-Velasco M., Zúñiga F.R., Valdés-González C.M. and Arámbula-Mendoza R.; 2021: *Spatial and temporal b-value characterization at Popocatépetl volcano, Central Mexico*. J. Volcanol. Geotherm. Res., 417, 107320.

Salah M.K., Sahin S. and Destici C.; 2007: *Seismic velocity and Poisson's ratio tomography of the crust beneath southwest Anatolia: an insight into the occurrence of large earthquakes.* J. Seismol., 11, 415-432.

Sandron D., Rebez A., Tamaro A. and Slejko D.; 2023: *Recent earthquakes (2000–2021) in and around the Friuli Venezia Giulia region (NE Italy) and quality improvements of the OGS network monitoring capabilities.* Bull. Geophys. Ocean., 64, 237-258.

Sarı C., Kamacı Z., Yağmurlu F., Timur E., Şentürk M. and Bozcu M.; 2023: *Paleoseismological features and tectonic setting of the Fethiye-Burdur Fault Zone (SW Turkey).* Geol. Anali Balk. Poluostrva, 84, 117-131.

Scholz C.H.; 1968: *The frequency-magnitude relation of microfracturing in rock and its relation to earthquakes.* Bull. Seismol. Soc. Am., 58, 399-415.

Scholz C.H.; 2015: *On the stress dependence of the earthquake b-value.* Geophys. Res. Lett., 42, 1399-1402.

Schorlemmer D., Wiemer S. and Wyss M.; 2004: *Earthquake statistics at Parkfield: 1. Stationarity of b-values.* J. Geophys. Res. Solid Earth, 109, B12307.

Schorlemmer D., Wiemer S. and Wyss M.; 2005: *Variations in earthquake-size distribution across different stress regimes.* Nature, 437, 539-542.

Shelly D.R., Hardebeck J.L., Ellsworth W.L. and Hill D.P.; 2016: *A new strategy for earthquake focal mechanisms using waveform-correlation-derived relative polarities and cluster analysis: Application to the 2014 Long Valley Caldera earthquake swarm.* J. Geophys. Res. Solid Earth, 121, 8622-8641.

Shi Y. and Bolt B.A.; 1982: *The standard error of the magnitude-frequency b-value.* Bull. Seismol. Soc. Am., 72, 1677-1687.

Sobiesiak M.M.; 2000: *Fault plane structure of the Antofagasta, Chile earthquake of 1995.* Geophys. Res. Lett., 27, 577-580.

Sobiesiak M., Meyer U., Schmidt S., Götze H.J. and Krawczyk C.M.; 2007: *Asperity generating upper crustal sources revealed by b-value and isostatic residual anomaly grids in the area of Antofagasta, Chile.* J. Geophys. Res. Solid Earth, 112, B12308.

Şaroğlu F., Emre Ö. and Kuşçu I.; 1992: *Türkiye Diri Fay Haritası (Active Fault Map of Turkey), 2 sheets.* General Directorate of Mineral Research and Exploration (MTA), Ankara, Turkey.

Şengör A.M.C., Görür N. and Şaroğlu F.; 1985: *Strike-slip faulting and related basin formation in zones of tectonic escape: Turkey as a case study.* In: Biddle K.T. and Christie-Blick N. (eds), Strike-Slip Deformation, Basin Formation, and Sedimentation. SEPM Spec. Publ., 37, 227-264.

Tan O., Tapırdamaz M.C. and Yörük A.; 2008: *The earthquake catalogues for Turkey*. Turk. J. Earth Sci., 17, 405-418.

Tan O.; 2020: *A Homogeneous Earthquake Catalogue for Turkey and Surrounding Region.* Nat. Hazards Earth Syst. Sci. Discuss., 2020, 1-23.

Taymaz T., Jackson J. and McKenzie D.; 1991: *Active tectonics of the north and central Aegean Sea.* Geophys. J. Int., 106, 433-490.

Taymaz T. and Price S.; 1992: The 1971 May 12 Burdur earthquake sequence, SW Turkey: a synthesis of seismological and geological observations. Geophys. J. Int., 108, 589–603.

Taymaz T., Yilmaz Y. and Dilek Y.; 2007: *The geodynamics of the Aegean and Anatolia: introduction*. Geol. Soc. London Spec. Publ., 291, 1-16.

Tormann T., Wiemer S. and Mignan A.; 2014: *Systematic survey of high-resolution b-value imaging along Californian faults: Inference on asperities*. J. Geophys. Res. Solid Earth, 119, 2029-2054.

Tosun L., Avşar U., Avşar Ö., Dondurur D. and Kaymakcı N.; 2021: *Active tectonics and kinematics of Fethiye-Göcek Bay, SW Turkey: insight about the eastern edge of Pliny-Strabo Trenches*. J. Struct. Geol., 145, 104287.

Türe O., Çobanoğlu İ., Gül M. and Karacan E.; 2021: *Seismic record approach for the evaluation of natural hazards: a key study from SW Anatolia/Turkey.* Environ. Earth Sci., 80, 500.

Utsu T.; 1966: *A statistical significance test of the difference in b-value between two earthquake groups*. J. Phys. Earth, 14, 37-40.

Utsu T., Ogata Y. and Matsuura R.S.; 1995: *The centenary of the Omori formula for decay law of aftershock activity.* J. Phys. Earth, 43, 1-33.

Warren N.W. and Latham G.V.; 1970: *An experimental study of thermally induced microfracturing and its relation to volcanic seismicity*. J. Geophys. Res., 75, 4455-4464.

Wiemer S. and McNutt S.R.; 1997: *Variations in the frequency magnitude distribution with depth in two volcanic areas: Mount St. Helens, Washington, and Mt. Spurr, Alaska.* Geophys. Res. Lett., 24, 189-192.

Wiemer S. and Wyss M.; 1997: *Mapping the frequency-magnitude distribution in asperities: An improved technique to calculate recurrence times?* J. Geophys. Res. Solid Earth, 102, 15115-15128.

Wiemer S. and Wyss M.; 2000: *Minimum magnitude of completeness in earthquake catalogs: Examples from Alaska, the western United States, and Japan.* Bull. Seismol. Soc. Am., 90, 859-869.

Wiemer S.; 2001: *A software package to analyze seismicity: ZMAP.* Seismol. Res. Lett., 72, 373-382.

Woessner J. and Wiemer S.; 2005: *Assessing the quality of earthquake catalogues: Estimating the magnitude of completeness and its uncertainty.* Bull. Seismol. Soc. Am., 95, 684-698.

Wu Y.M. and Chiao L.Y.; 2006: *Seismic quiescence before the 1999 Chi-Chi, Taiwan, Mw 7.6 earthquake.* Bull. Seismol. Soc. Am., 96, 321-327.

Wu Y.M., Chen C.C., Zhao L. and Chang C.H.; 2008: *Seismicity characteristics before the 2003 Chengkung, Taiwan, earthquake.* Tectonophysics, 457, 177-182.

Wu Y.M., Chen S.K., Huang T.C., Huang H.H., Chao W.A. and Koulakov I.; 2018: *Relationship between earthquake b-values and crustal stresses in a young orogenic belt.* Geophys. Res. Lett., 45, 1832-1837.

Wyss M.; 1973: T*owards a physical understanding of the earthquake frequency distribution*. Geophys. J. R. Astron. Soc., 31, 341-359.

Wyss M., Hasegawa A., Wiemer S. and Umino N.; 1999: *Quantitative mapping of precursory seismic quiescence before the 1989, M 7.1 off-Sanriku earthquake, Japan.* Ann. Geophys., 42(5).

Wyss M., Schorlemmer D. and Wiemer S.; 2000: *Mapping asperities by minima of local recurrence time: San Jacinto-Elsinore fault zones.* J. Geophys. Res. Solid Earth, 105, 7829-7844.

Yolsal-Çevikbilen S., Taymaz T. and Helvacı C.; 2014: *Earthquake mechanisms in the Gulfs of Gökova, Sığacık, Kuşadası, and the Simav Region (western Turkey): Neotectonics, seismotectonics and geodynamic implications.* Tectonophysics, 635, 100-124.

Corresponding author: Tekin Yeken
Hereke Asım Kocabıyık Vocational School, Construction Technology Programme, Kocaeli University,
Agah Ateş Mahallesi, Cumhuriyet Caddesi No: 47 41800 Hereke, Körfez, Kocaeli, Turkey
Phone +902627423290; e-mail: tyeken@kocaeli.edu.tr

SUPPLEMENTARY MATERIALS

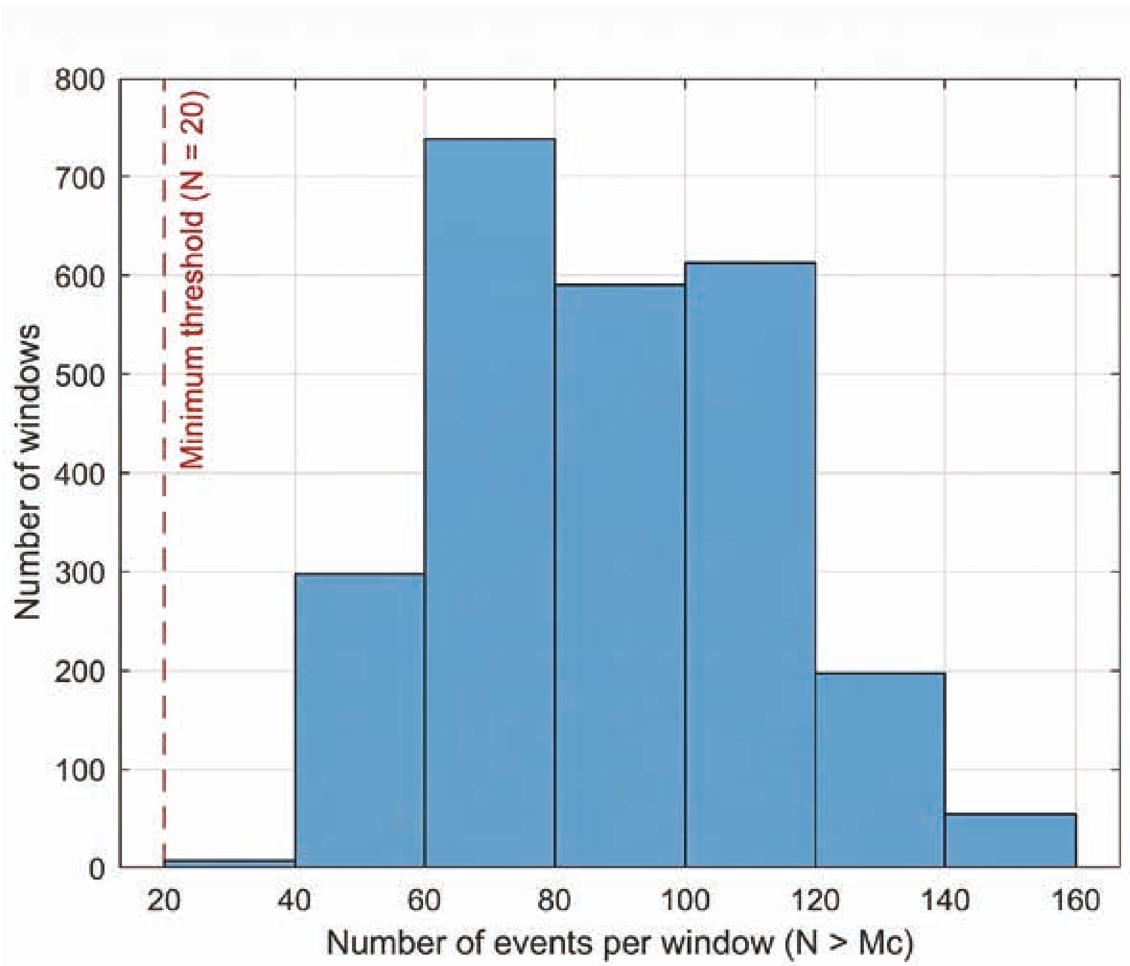

Fig. S1 - Histogram showing the distribution of the number of earthquakes per sliding time window used in the temporal *b*-value analysis (events with $M \geq Mc$). The red dashed line marks the minimum threshold of 20 events. Although this value defines the lower bound, the majority of windows contain substantially more events, typically between ~50 and 120, indicating that most *b*-value estimates are based on statistically more robust samples than the minimum threshold.

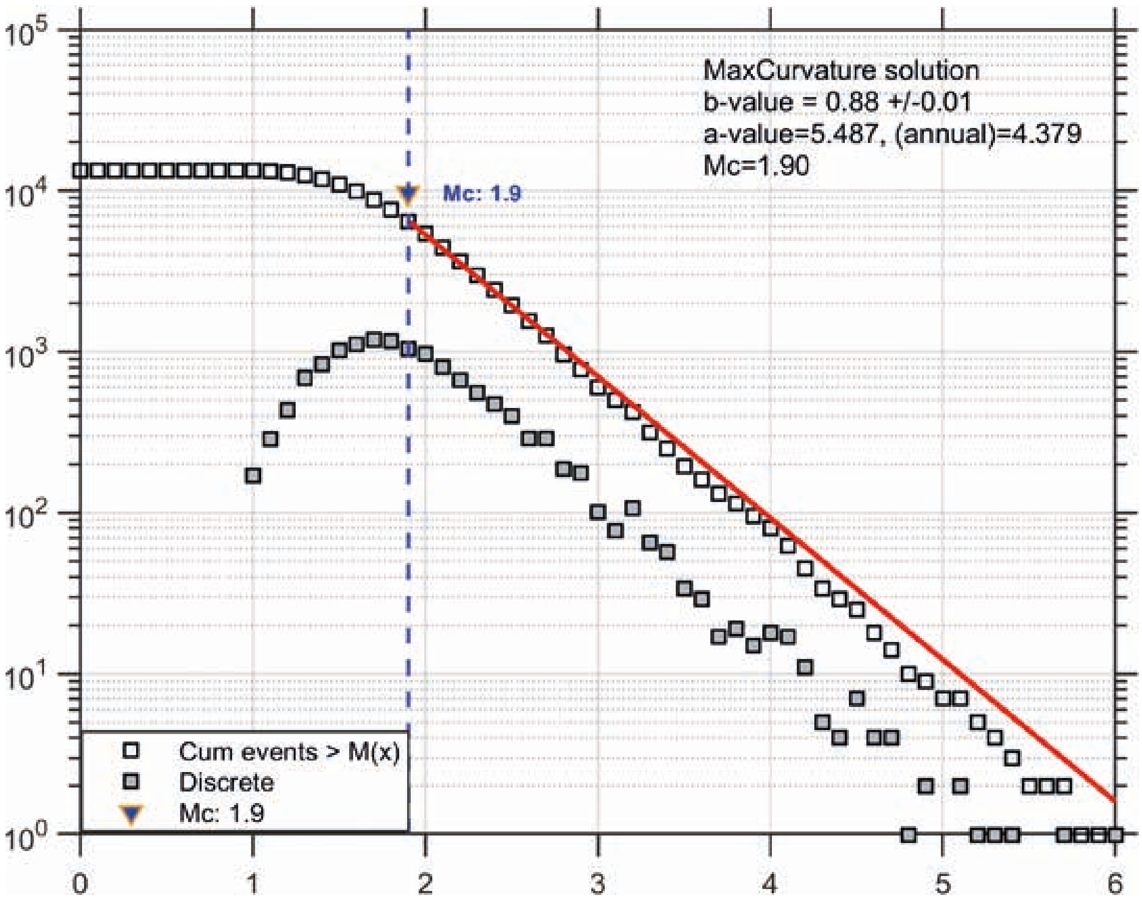

Fig. S2 - Application of a +0.2 unit correction to the *Mc* in the 2012–2024 raw catalogue significantly improved the fit of the FMD. This adjustment, implemented following the methodology of Woessner and Wiemer (2005), effectively compensated for the observed overestimation at $M \geq 3.0$, yielding a more robust linear relationship across the complete magnitude range. The a-value is reported as an annualised seismicity rate, normalised to one year of observation.